JOURNAL OF SPACECRAFT AND ROCKETS
Vol. 36, No. 1, January–February 1999

Computation of Roll Moment for Projectile with Wraparound Fins Using Euler Equation

Seung-Kil Paek,* Tae-Sang Park,* Jae-Sung Bae,* In Lee,† and Jang Hyuk Kwon‡
Korea Advanced Institute of Science and Technology, Taejon 305-701, Republic of Korea

Flowfield solutions of a projectile with wraparound fins have been computed in a supersonic region with a time-marching, three-dimensional Euler equation. The roll moment coefficients were computed from the flowfield solution and compared with the experimental results. The roll moment coefficient computations show good agreement with the experimental measurements for various flight Mach numbers. This shows that the Euler equations can give comparably accurate solutions when computing the roll moment of wraparound fin configurations. Comparing the flowfield solutions before and after the roll reversal, the roll reversal at higher Mach number than Mach 1 is thought to be due to the effect of a compression/expansion wave from a neighboring fin. Through the comparison with the previous results, it is shown that the tip shape, as well as the edge shape, has a significant effect on the roll moment of the wraparound fin.

Nomenclature

A_{ref}	= reference area, $\pi D^2/4$
C_l	= roll moment coefficient, $L/\frac{1}{2}\rho_\infty U_\infty^2 D A_{\text{ref}}$
D	= reference length, the diameter of the projectile body, 1.524 cm
$\hat{E}, \hat{F}, \hat{G}$	= contravariant flux vectors in generalized coordinates
e	= total energy, nondimensionalized by U_∞^2
h	= enthalpy, nondimensionalized by U_∞^2
J	= Jacobian
L	= roll moment, whose positive direction is from nose to tail
M_∞	= freestream Mach number
p	= pressure, nondimensionalized by $\rho_\infty U_\infty^2$
p_∞	= freestream static pressure
$\hat{Q}$	= conservative flow variable vector
T_ξ, T_η, T_ζ	= eigenvector matrices of flux Jacobian along the generalized coordinates
U_∞	= freestream flow speed
U, V, W	= contravariant velocities along the generalized coordinates
u, v, w	= Cartesian velocity components, nondimensionalized by U_∞
x, y, z	= Cartesian coordinates, nondimensionalized by D
$\hat{\Lambda}_\xi, \hat{\Lambda}_\eta, \hat{\Lambda}_\zeta$	= eigenvalue vectors of flux Jacobian along the generalized coordinates
ξ, η, ζ	= generalized coordinates
ρ	= density, nondimensionalized by ρ_∞
ρ_∞	= freestream density

Introduction

WRAPAROUND fins, which are curved in the spanwise direction, have been used primarily for their advantages in packing tube-launched projectiles during the past few decades. These surfaces can fold against the cylindrical projectile body and be made to fit into the launch tube, allowing more efficient use of space. Thus, a larger number of wraparound fin projectiles can be stored in the same space as fixed-fin projectiles designed to deliver the same payload. These wraparound fin configurations have conventional longitudinal aerodynamic characteristics similar to those of configurations with planar fins of identical planform.[1] However, aerodynamic anomalies exist in the form of a roll moment at zero angle of attack, a roll reversal near Mach 1, and the presence of a side force/moment at a nonzero angle of attack.[2] The phenomenon that the sign of the roll moment changes as the Mach number increases is known as roll reversal. To design dynamically stable projectiles employing wraparound fins, it is necessary to have the ability to predict the roll moment coefficient accurately at all of the flight conditions for the full trajectory. Conventional empirical or semi-empirical analysis tools have not predicted the roll moments with wraparound fin configurations accurately.

Previous research has been conducted to compute the roll moment of wraparound fin configurations using analytical methods. Bar-Haim and Seginer[3] computed roll characteristics in the subsonic region with lifting-line theory and prescribed wake modeling based on experimental data. Though the comparison with experimental data is very accurate and impressive, the method used is limited to the subsonic flow region and can be classified as a semi-empirical method. Recently, some research has been devoted to compute the roll moment of wraparound fins with computational fluid dynamics (CFD).[4,5] These CFD studies of missile configurations with wraparound fins have shown general agreement with experimental data but always lacked the accuracy in roll moment and side force/moment determination. Edge[6] calculated the roll moment for a laminar flow case with a three-dimensional full Navier–Stokes code. In his paper, he made a comment that the inviscid aerodynamic modeling in the previous studies might have been the main cause of the failures in computing roll moment. There may be, however, another cause that is as important as viscosity: improper fin geometry modeling. Recently, Abate and Cook[7] calculated the roll moment of wraparound fins attached to an infinitely long cylinder using an Euler code. They indicated that the roll moment did not appear if the fin thickness was neglected. The accuracy of the CFD results greatly depends on how accurately the configuration is modeled. The previous researchers had approximated the tip shape[4] or neglected the thickness of the fins[5] because the detailed modeling of the wraparound fin geometry is somewhat difficult in the grid construction. The longitudinal aerodynamic characteristics are computed accurately only if the planform is accurately modeled, even though the fin geometry is approximated. The shape of the wing tip is often approximated for conventional wings, but it is important to model the fin shape as accurately as possible because the aerodynamic properties are heavily dependent on the wraparound fin geometry. The concern of the present paper is to demonstrate that accurate fin geometry modeling is important, and that the edge

Received Oct. 23, 1997; revision received Aug. 1, 1998; accepted for publication Sept. 10, 1998. Copyright © 1998 by the American Institute of Aeronautics and Astronautics, Inc. All rights reserved.

*Graduate Research Assistant, Department of Aerospace Engineering, 373-1 Kusong-dong, Yusong-gu.

†Professor, Department of Aerospace Engineering, 373-1 Kusong-dong, Yusong-gu. Senior Member AIAA.

‡Associate Professor, Department of Aerospace Engineering, 373-1 Kusong-dong, Yusong-gu. Member AIAA.

and tip shapes give significant changes in the roll moment of the wraparound fin configuration.

Formulation

The Euler equations in strong conservative form for a generalized coordinate system are given as

$$\frac{\partial \hat{Q}}{\partial \tau} + \frac{\partial \hat{E}}{\partial \xi} + \frac{\partial \hat{F}}{\partial \eta} + \frac{\partial \hat{G}}{\partial \zeta} = 0 \tag{1}$$

where the conservative variable $\hat{Q}$ and the flux vectors $\hat{E}$, $\hat{F}$, and $\hat{G}$ are

$$\hat{Q} = J^{-1}\lfloor \rho \quad \rho u \quad \rho v \quad \rho w \quad \rho e \rfloor^T \tag{2}$$

$$\hat{E} = \lfloor \rho U \quad \rho u U + \xi_x p \quad \rho v U + \xi_y p \quad \rho w U + \xi_z p \quad \rho U h \rfloor^T$$

$$\hat{F} = \lfloor \rho V \quad \rho u V + \eta_x p \quad \rho v V + \eta_y p \quad \rho w V + \eta_z p \quad \rho V h \rfloor^T$$

$$\hat{G} = \lfloor \rho W \quad \rho u W + \zeta_x p \quad \rho v W + \zeta_y p \quad \rho w W + \zeta_z p \quad \rho W h \rfloor^T \tag{3}$$

where

$$U = \xi_x u + \xi_y v + \xi_z w, \qquad V = \eta_x u + \eta_y v + \eta_z w$$
$$W = \zeta_x u + \zeta_y v + \zeta_z w \tag{4}$$

The pressure p and enthalpy h can be related to the dependent variables by applying the ideal gas law:

$$p = \rho(\gamma - 1)\left\lfloor e - \tfrac{1}{2}(u^2 + v^2 + w^2)\right\rfloor \tag{5}$$

$$h = e + p/\rho \tag{6}$$

For a numerical implementation, we used the finite volume method for the spatial discretization and the diagonally approximate factorization method[8] for the time integration. The final form of the Euler equation is

$$T_\xi \lfloor I + \Delta\tau\delta_\xi \hat{\Lambda}_\xi \rfloor \left(T_\xi^{-1} T_\eta\right) \lfloor I + \Delta\tau\delta_\eta \hat{\Lambda}_\eta \rfloor \left(T_\eta^{-1} T_\zeta\right)$$
$$\times \lfloor I + \Delta\tau\delta_\zeta \hat{\Lambda}_\zeta \rfloor \left(T_\zeta^{-1}\right) \Delta\hat{Q} = \hat{R} \tag{7}$$

$$\hat{R} = -\Delta\tau(\delta_\xi \hat{E} + \delta_\eta \hat{F} + \delta_\zeta \hat{G}) \tag{8}$$

where $\hat{\Lambda}$ and T are available in Ref. 8. The following flux-vector-splitting method is applied to maintain the matrices scalar tridiagonal and simultaneously to upwind the eigenvalue difference:

$$I + \Delta\tau\delta_\xi \hat{\Lambda}_\xi = \left\lfloor -\tfrac{1}{2}\Delta\tau(\hat{\Lambda} + |\hat{\Lambda}|)\right\rfloor_{i-1} + \lfloor I + \Delta\tau|\hat{\Lambda}|\rfloor_i$$
$$+ \left\lfloor \tfrac{1}{2}\Delta\tau(\hat{\Lambda} - |\hat{\Lambda}|)\right\rfloor_{i+1} \tag{9}$$

The implicit terms of Eq. (7) are all scalar tridiagonal matrices, so that the computation time is much smaller than Beam and Warming's method,[9] which solves block tridiagonal matrices. Though the time accuracy is reduced to first order, it still gives accurate steady-state solutions.

The flux difference terms of Eq. (8) are computed by a second-order total variation diminishing (TVD) scheme.[10] The second-order TVD fluxes are constructed, for example, in the ξ direction, as

$$\hat{F}_{i+\frac{1}{2}} = \tfrac{1}{2}(\hat{F}_i + \hat{F}_{i+1}) + \tfrac{1}{2}\left[J^{-1} T_\xi \Phi_\xi\right]_{i+\frac{1}{2}} \tag{10}$$

where Φ is the dissipative term to satisfy the TVD conditions, the component of which is given by

$$\Phi^l_{i+\frac{1}{2}} = -\Psi\left(\hat{\Lambda}^l_{i+\frac{1}{2}}\right)\left[\alpha^l_{i+\frac{1}{2}} - g^l_{i+\frac{1}{2}}\right] \tag{11}$$

where Ψ is the function required to prevent nonphysical solutions such as expansion shocks. The various α are spatial differences of the characteristic variables, the various g are limiter functions, and the following van Leer limiter is used in this study:

$$g^l_{i+\frac{1}{2}} = \frac{\alpha^l_{i+\frac{1}{2}}\alpha^l_{i-\frac{1}{2}} + \left|\alpha^l_{i+\frac{1}{2}}\alpha^l_{i-\frac{1}{2}}\right|}{\alpha^l_{i+\frac{1}{2}} + \alpha^l_{i-\frac{1}{2}}} \tag{12}$$

Experimental Comparison Data

A standard wraparound fin projectile designed by The Technical Cooperation Program (TTCP), as seen in Fig. 1, was used as the basic configuration for the computation.[6,11] This TTCP configuration has fins with symmetric leading- and trailing-edge bevels. Note that a difference of 45 deg exists between the root and tip chord cross section. The detailed fin geometry is shown in Fig. 2. All dimensions are expressed in units of calibers (1 caliber = 1.524 cm). The experimental data were obtained from an experiment conducted at the Jet Propulsion Laboratory, California Institute of Technology, (JPL). The test model is a scaled-down version of the original TTCP standard configuration (1 caliber = 10.16 cm). For the TTCP standard configuration, there are different roll moment coefficients obtained from the wind-tunnel tests at various facilities, such as the McDonnell Douglas Aerophysics wind tunnel, the Arnold Engineering Development Center, and NASA Langley Research Center. Although the models used at JPL did not have any boundary-layer trips, other wind-tunnel test models were reported to have boundary-layer trips on the fin leading edges.[6,11] Because the Euler equations cannot predict viscous effects, the roll moment coefficients from JPL have been compared with the values computed from the flowfield solutions by the present Euler code. Figure 3 is the computational model used by Edge.[6] His computational model has blunt leading and trailing edges, and the root and tip chord cross sections are parallel in the computational model. The roll moment computation for this model will be used later for a comparison.

Results and Discussion

The computational domain was taken to be the region including the upper surface (concave side) of one fin and the lower surface (convex side) of the adjacent fin as the outer boundaries of the domain. This region is referred to here as a fin passage. In general, to

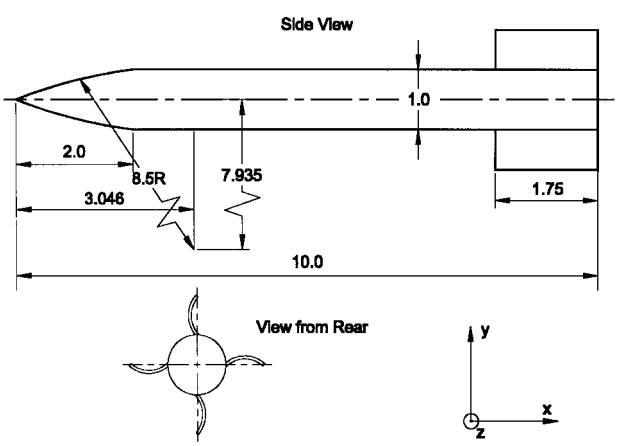

Fig. 1 Geometry of the TTCP standard model.

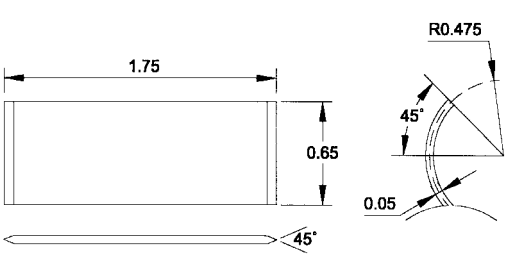

Fig. 2 Fin shape of the TTCP standard model.

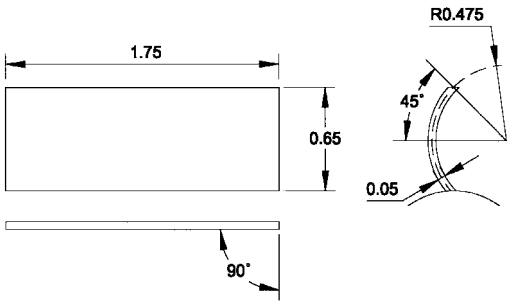

Fig. 3 Fin shape of the computational model used by Edge.[6]

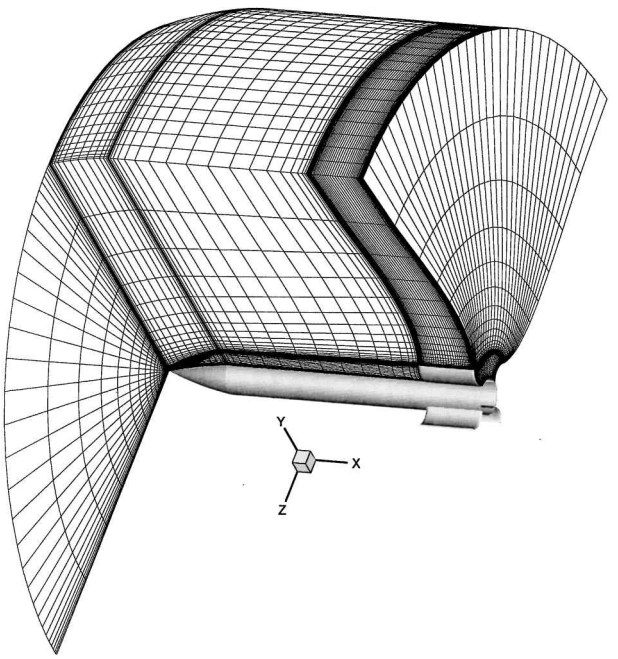

Fig. 4a Computational grid (108 × 33 × 57, 65 × 9 × 11, and 65 × 9 × 11).

model the influence of adjacent fins, the entire projectile with all of the fins would need to be solved. However, for an axisymmetric flowfield considered here, all fin passages can be assumed to be identical, and only one fin passage needs to be solved with the conditions of symmetry. The grid system used consists of three blocks. One block is for the fin passage, and two blocks are for the region around the fin tip. The dimensions for the three blocks are (108 × 33 × 57), (65 × 9 × 11), and (65 × 9 × 11), respectively. These grid dimensions are selected to make insignificant changes in flowfield solutions if they become doubled (as is shown in Fig. 4). Figure 4b shows the grid geometry around the wraparound fin. The geometry of the TTCP standard model is accurately reflected. The flowfield solutions were computed at various Mach number from 1.2 to 3.0.

Figure 5 shows the roll moment coefficient as a function of Mach number. Experimental data were obtained at JPL, and computations were made with the present Euler code. This figure shows that the roll moment coefficients computed with the present Euler code agree well with the trend and the magnitude of the experimental data. Note that the agreement is especially good at higher Mach numbers. The figure indicates that a crossover points or a Mach number at which the roll moment coefficient is zero, exists near Mach 1.8, which is almost the same as the experimental result. The trend that the roll moment curve has small peaks before and after the crossover point resembles the results obtained by Abate and Cook.[7] If the computational grid is prepared accurately, the Euler equations can give roll moment solutions with reasonable accuracy. Tilmann et al.[12] investigated the flow structure near a single wraparound fin at $M = 2.8$ experimentally and compared it with computations from an Euler code. They reported that many aspects of the flowfield around a wraparound fin were accurately captured by

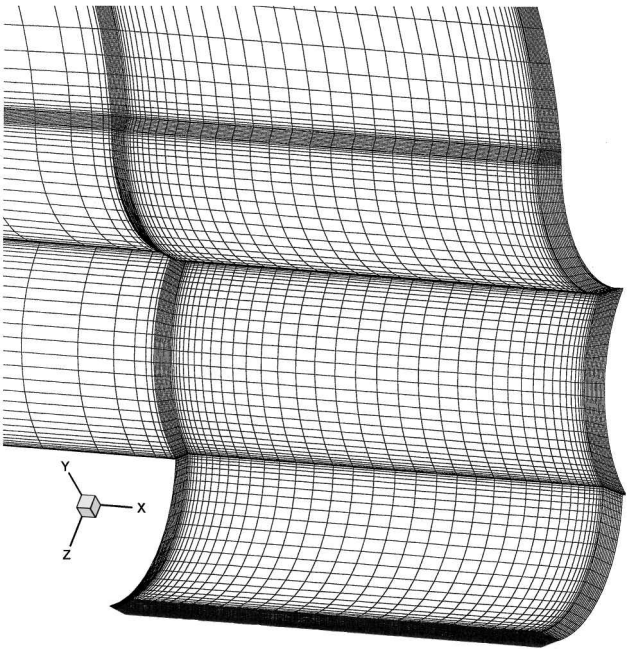

Fig. 4b Mesh in vicinity of the fin.

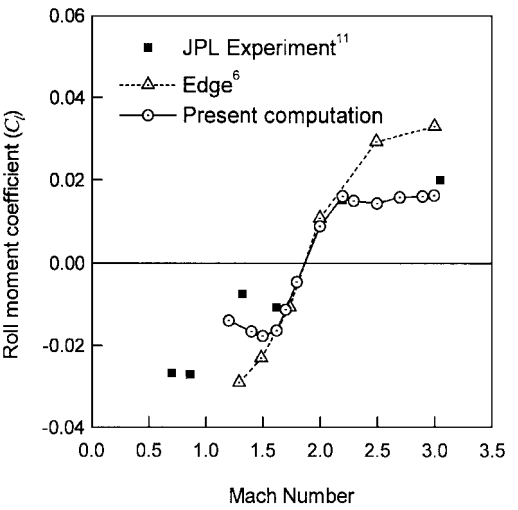

Fig. 5 Roll moment coefficient vs Mach number for computational and JPL experimental data.

the numerical solution. However, a viscous effect can be important in computing the roll moment of projectiles with wraparound fins. The present result by the Euler equation is confined to the region where the inviscid modeling is valid. In the wind-tunnel test results, the crossover points were somewhat different from the flight test result that were used for a comparison, and the roll moment coefficients were dependent on Reynolds number, if no explicit trends[11] were found. Hence, to predict roll moment coefficients that agree well with wind-tunnel test results, viscosity consideration may be needed. However, detailed geometry modeling is important in computing the roll moment of wraparound fins. Edge's results show a similar trend but have some discrepancy in magnitude. Though Edge used a full Navier–Stokes code, the flow was assumed to be laminar. Hence, the most significant difference with the present case is the edge and tip shape of the fin. As mentioned earlier, Edge's computational model has blunt leading and trailing edges, and the root and tip chord cross sections are parallel to each other.

Figure 6 shows surface pressure contours on the concave and convex sides of the wraparound fins at $M = 2.5$. This Mach number is selected to observe the pressure distributions after the crossover point. The roll moment at $M = 2.5$ has a positive value, as seen in Fig. 5. We can see the difference between the surface pressure contours on the convex and concave side. The compression or expansion

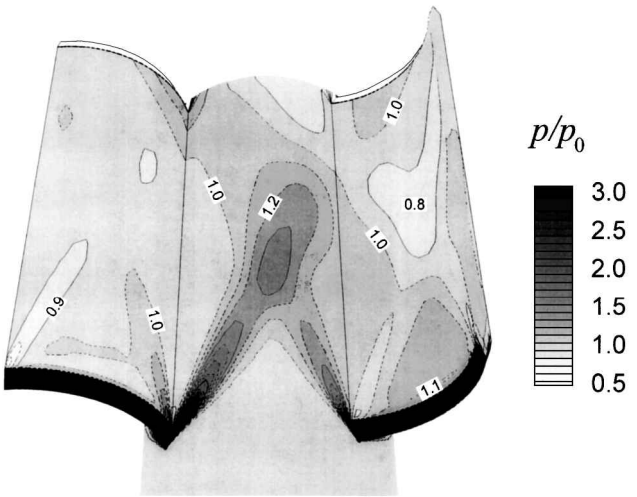

Fig. 6 Normalized pressure contours at $M = 2.5$.

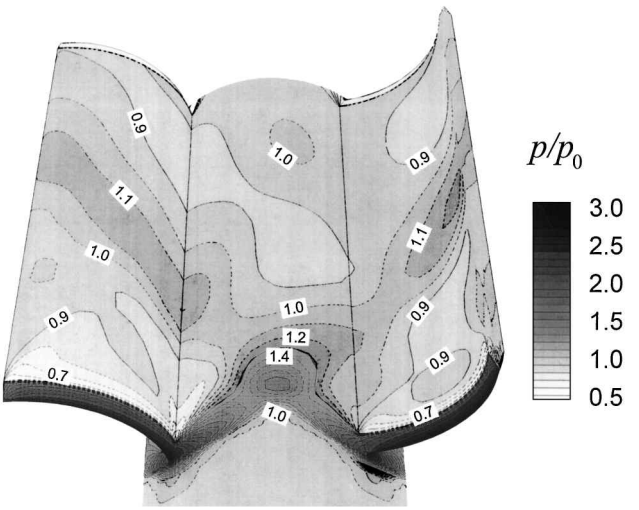

Fig. 8 Normalized pressure contours at $M = 1.5$.

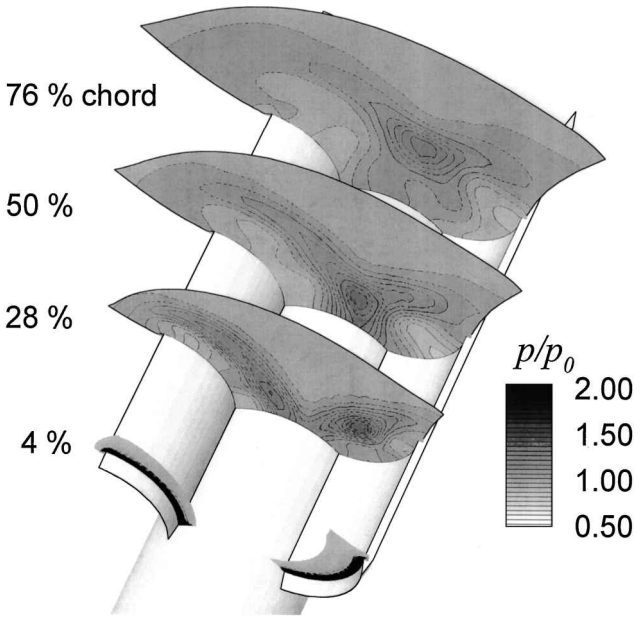

Fig. 7 Normalized pressure contours at various axial stations at $M = 2.5$.

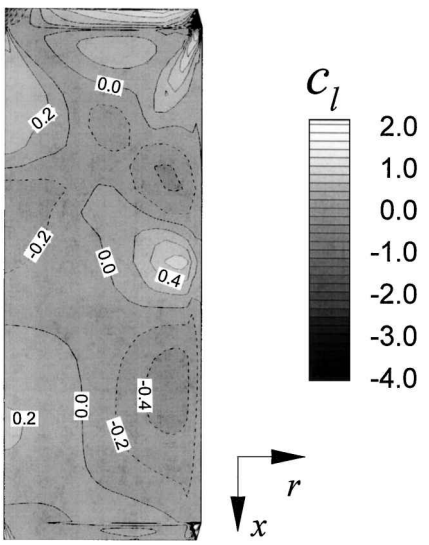

Fig. 9 Roll moment coefficient distribution at $M = 1.5$.

wave from the leading-edge root of one fin affects the pressure distribution on the rear region of the adjacent fin, but the affected region is small. It is concluded that the effect of each fin on the pressure distribution on the adjacent fin is small at $M = 2.5$. Figure 7 shows the pressure contours at various axial positions along the fin chord (4, 28, 50, and 76% of the chord length) at this Mach number. In this figure, the fin geometry is somewhat exaggerated: the dimension along the x axis is increased twice as large as those along y or z axis. The contours give a good indication of the overall structure of shocks generated by a wraparound fin projectile. A core of high pressure appears on the concave side, develops along the chord, merges with the core of somewhat lower pressure from the convex side at about 50% chord length, and proceeds rearward. Though this will be shown later, the movement of the pressure core coincides with the sectional roll moment coefficient distribution.

Figure 8 shows surface pressure contours on the concave and convex sides of the wraparound fins at $M = 1.5$. The roll moment at this Mach number has a negative value. The differences between the surface pressure distributions on the convex and concave side are quite prominent compared with those at $M = 2.5$. The compression or expansion wave from the leading-edge root of one fin affects the pressure distribution on the midregion of the adjacent fin. The effect of the wave from the leading-edge tip appears because the wave angle increases. The wave from the leading-edge tip of one fin also affects that on the rear region of the adjacent fin. Considering the wave angle or Mach angle, we can see that the pressure distribution over the entire fin surface at $M = 2.5$ is concentrated around only the leading edge of the fin at $M = 1.5$. It is thought that the roll reversal of this wraparound configuration appears when the effect of a compression or expansion wave from one fin on an adjacent fin decreases as Mach number increases. However, this is not the main cause of the roll moment generation at the angle of attack of 0 deg and roll reversal phenomena through Mach 1 for wraparound fin configurations because roll moments observed at subsonic speeds cannot be explained in this way. It is thought that roll reversal occurs because the characteristics of an asymmetric flowfield due to fin thickness and curvature change as the Mach number increases, which is explained by considering converging/diverging nozzle flow.[7] Roll reversal at Mach numbers above Mach 1 is due to the effect of a compression or an expansion wave.

Figures 9 and 10 show roll moment coefficient distribution on the radial plane resulting from the pressure difference between the convex and concave sides of the fin at $M = 1.5$ and 2.5, respectively. Integrating the distribution over the radial plane, the total roll moment coefficient can be obtained. The roll moment coefficient distribution at $M = 1.5$ is as complex as the pressure distribution, compared with that at $M = 2.5$. It is obvious that the roll moment distribution around the leading edge at $M = 1.5$ resembles that at $M = 2.5$, when the wave angle is considered. Figures 11 and 12 show the sectional roll moment coefficient along axial and radial direction, at $M = 1.5$ and 2.5, respectively. The sectional roll moment

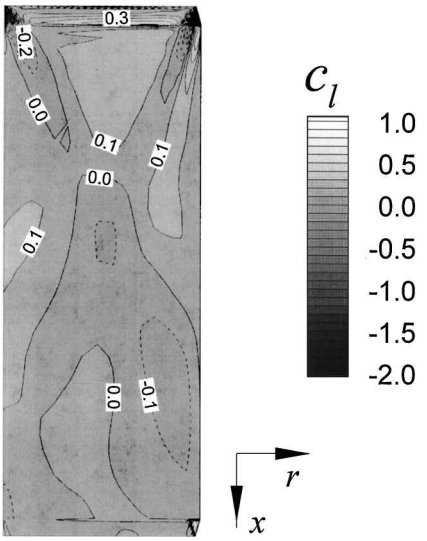

Fig. 10 Roll moment coefficient distribution at M = 2.5.

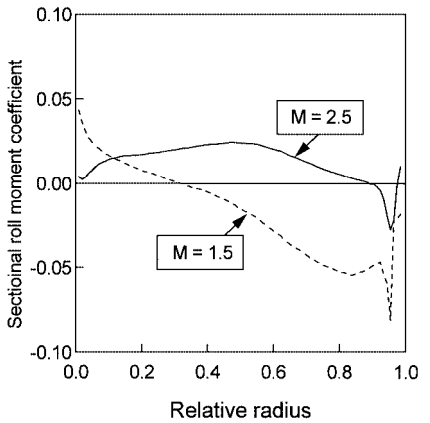

Fig. 11 Sectional roll moment coefficient along the radial direction.

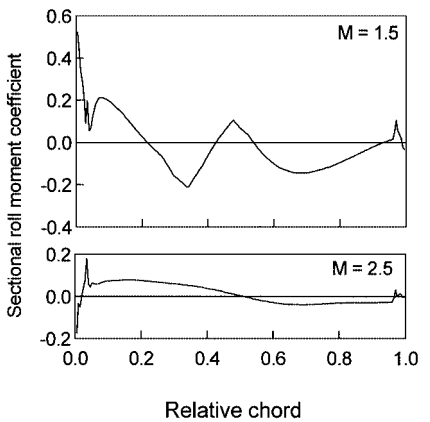

Fig. 12 Sectional roll moment coefficient along the axial direction.

coefficient in Fig. 11 is the sum of all of the roll moment coefficients produced at each radial position. The sectional roll moment coefficient in Fig. 12 is the sum of all of the roll moment coefficients produced at the same axial position. Note that in Fig. 11 the magnitude of the negative roll moment increases along the radial direction at $M = 1.5$. At $M = 2.5$, the sign of the sectional moment is maintained positive along the radial direction and changes negative around the tip. Hence, the signs of the moment coefficients around the tip region at both of the Mach numbers are all negative. This indicates that the tip produces negative roll moment. In Fig. 12, the sign of the sectional roll moment at $M = 1.5$ changes several times along the axial direction. This is due to the complex pressure distribution resulting from the alternating compression/expansion phenomenon along the chord (see Fig. 9). Some fluctuation is seen around the leading and trailing edges. This is due to the beveled shapes of the leading and trailing edges. The trend of the sectional roll moment distribution along the chord at $M = 2.5$ is much simpler and, although the magnitude is smaller, is nearly the same as that around the leading edge at $M = 1.5$. As mentioned earlier, the change of the sectional roll moment coefficient coincides with the movement of the pressure core at $M = 2.5$. A positive moment coefficient appears and grows in the leading-edge region, and the sign of the moment coefficient changes to negative along the chord direction. The reason why the pressure difference or the roll moment is larger at the lower Mach number is the fact that the effect of the curvature increases because of larger wave angle.

The pressure distributions shown in Figs. 6–8 resemble the results obtained by Edge.[6] It is thought that the moment distributions on the fin surface also will have nearly the same trend. However, the computed roll moments have some discrepancies in magnitude. It is only due to the geometric difference between two models: edge and fin tip shape. As seen in Figs. 11 and 12, the roll moment fractions produced in these regions are comparatively large. In Edge's model, the tip chord cross section is parallel to the root chord cross section and the area projected to the radial plane is negligible. Hence, the effect of the roll moment produced around the tip is thought to be smaller. In the present model, because the tip chord cross section forms an angle of 45 deg with the root chord cross section, the area projected to the radial plane cannot be neglected. The pressure on the tip chord cross section makes a considerable contribution to the total roll moment.

The edge and tip shapes may have a great significance in roll moment of wraparound fins, and even the Euler equations can give roll moment solutions with a comparable accuracy.

Conclusions

Flowfield solutions of a wraparound fin projectile were calculated with the three-dimensional Euler equations. Computational grids were constructed to reflect accurately the fin edge shape of the experimental model. The roll moment coefficient was calculated from the flowfield solutions and compared with the roll moment coefficient obtained from experimental measurements. The computed roll moment coefficients showed good agreement with the experimental results in magnitude and sign. That means that if the computational grid is prepared accurately the Euler equations can give roll moment solutions with a comparable accuracy.

The roll reversal of a wraparound configuration generally occurs around Mach 1, but in the present case, it occurred at $M = 1.8$. It is observed that the effect on the adjacent fin of the compression or expansion wave from the tip of one fin is comparatively large at the Mach numbers below the roll reversal point and that it decreases as Mach number increases. From this it is thought that the effect of the compression or expansion wave delays the roll reversal toward higher Mach number. Through the comparison with the results of another wraparound fin configuration with different edge and tip shapes, it is shown that the roll moment of the wraparound fin is significantly affected by the edge and tip shapes.

Acknowledgment

The work presented in this article was supported by the Agency for Defense Development in Korea. This support is gratefully acknowledged.

References

[1]Lucero, E. F., "Subsonic Stability and Control Characteristics of Configurations Incorporating Wrap-Around Surfaces," *Journal of Spacecraft and Rockets*, Vol. 13, No. 12, 1976, pp. 740–745.

[2]Winchenbach, G. L., Buff, R. S., Whyte, R. H., and Hathaway, W. H., "Subsonic and Transonic Aerodynamics of a Wraparound Fin Configuration," *Journal of Guidance, Control, and Dynamics*, Vol. 9, No. 6, 1986, pp. 627–632.

[3]Bar-Haim, B., and Seginer, A., "Aerodynamics of Wraparound Fins," *Journal of Spacecraft and Rockets*, Vol. 20, No. 4, 1983, pp. 339–344.

[4]Wardlaw, A. B., Priolo, F. J., and Solomon, J. M., "Multiple-Zone Strategy for Supersonic Missiles," *Journal of Spacecraft and Rockets*, Vol. 24, No. 4, 1987, pp. 377–384.

[5]Vitale, R. E., Abate, G. L., Winchenbach, G. L., and Riner, W., "Aerodynamic Test and Analysis of a Missile Configuration with Curved Fins," AIAA Paper 92-4495, Aug. 1992.

[6]Edge, H. L., "Computation of the Roll Moment for a Projectile with Wrap-Around Fins," *Journal of Spacecraft and Rockets*, Vol. 31, No. 4, 1994, pp. 615–620.

[7]Abate, G. L., and Cook, T., "Analysis of Missile Configurations with Wrap-Around Fins Using Computational Fluid Dynamics," AIAA Paper 93-3631, Aug. 1993.

[8]Pulliam, T. H., and Chaussee, D. S., "A Diagonal Form of an Implicit Approximate Factorization Algorithm," *Journal of Computational Physics*, Vol. 39, No. 2, 1981, pp. 347–363.

[9]Beam, R. M., and Warming, R. F., "An Implicit Finite Difference Algorithm for Hyperbolic Systems in Conservative-Law Form," *Journal of Computational Physics*, Vol. 22, 1976, pp. 87–110.

[10]Park, T. S., and Kwon, J. H., "An Improved Multistage Time Stepping for Second-Order Upwind TVD Schemes," *Computers and Fluids*, Vol. 7, 1996, pp. 629–645.

[11]Dahlke, C. W., "The Aerodynamic Characteristics of Wrap-Around Fins at Mach Numbers of 0.3 to 3.0," U.S. Army Missile Command, TR RD-77-4, Redstone Arsenal, AL, Oct. 1976.

[12]Tilmann, C. P., Huffman, R. E., Jr., Buter, T. A., and Bowersox, R. D. W., "Experimental Investigation of the Flow Structure near a Single Wraparound Fin," *Journal of Spacecraft and Rockets*, Vol. 34, No. 6, 1997, pp. 729–736.

R. M. Cummings
Associate Editor